

RSC Advances



This is an *Accepted Manuscript*, which has been through the Royal Society of Chemistry peer review process and has been accepted for publication.

Accepted Manuscripts are published online shortly after acceptance, before technical editing, formatting and proof reading. Using this free service, authors can make their results available to the community, in citable form, before we publish the edited article. This *Accepted Manuscript* will be replaced by the edited, formatted and paginated article as soon as this is available.

You can find more information about *Accepted Manuscripts* in the [Information for Authors](#).

Please note that technical editing may introduce minor changes to the text and/or graphics, which may alter content. The journal's standard [Terms & Conditions](#) and the [Ethical guidelines](#) still apply. In no event shall the Royal Society of Chemistry be held responsible for any errors or omissions in this *Accepted Manuscript* or any consequences arising from the use of any information it contains.

Viscoelasticity of wood cell walls with different moisture content as measured by nanoindentation

Yujie Meng^a, Yuzhi Xia^{b,c}, Timothy M. Young^a, Zhiyong Cai^d, Siqun Wang^{a*}

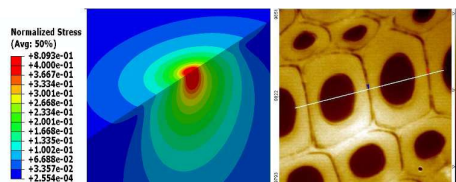
Received 00th January 20xx,
Accepted 00th January 20xx

DOI: 10.1039/x0xx00000x

www.rsc.org/

Instrumental indentation was performed on wood cell walls to measure the cell walls' mechanical properties and creep behaviour over a range of various steady moisture conditions. The wood cell walls' Young's modulus and hardness of were found negatively correlated with moisture content. Theoretical modeling

with Burgers model and finite element analysis with the Generalized Maxwell model were used to simulate the process of nanoindentation separately and to gain insight into the response of viscoelastic materials. Young's modulus extracted from Burgers model was lower than that from Generalized Maxwell model and Oliver-Pharr method, indicating that creep happened during indentation loading process. The extracted parameters from both models exhibited negative trends with increasing moisture contents. Both models confirmed an intuitive understanding of creep in viscoelastic wood cell wall, which reflects previous basic information about the composite structure of wood cell walls and their rheological properties.



Introduction

Nanoindentation has been demonstrated to be an effective analytical technique for measuring the small scale mechanical properties of biomass, with materials widely range from grass¹⁻³, crop stalks^{4, 5}, wood⁶⁻⁸, bamboo⁹, Lyocell fiber¹⁰, lignocelluloses¹¹ and so forth. Generally, the Young's modulus and hardness obtained from commercial instruments are extracted by the approach of Oliver and Pharr method, which is based on the assumption that the unloading curve is pure elastic¹². In cases where materials have time-dependent behaviour (i.e. viscoelasticity), rather than elastic-plastic in Oliver and Pharr's paper, creep occurs during nanoindentation unloading where the continuous increase of displacement at the onset of unloading and

the value of Young's modulus will be lower than the real instantaneous one ($t=0s$). This has been ascribed to internal friction stress opposing slip¹³. An extreme case of a viscoelastic material's response is the presence of a "nose" shape on unloading curves, resulting in either an overestimation of Young's modulus or negative contact stiffness as measured by Oliver and Pharr's method. Common ways to overcome the effect of creep include allowing sufficient creep time and removing the creep effect on contact stiffness and contact area during data analysis.

Viscoelasticity can be described as a combination of viscous components and simultaneously elastic behaviour. Attempts have been made using several models to link nanoindentation test data to meaningful mechanical properties of viscoelastic material¹⁴. Radok et al. developed an analytical solution for a viscoelastic model based on a principle between elasticity and linear viscoelasticity, but limited the validity by positing a constant contact area¹⁵. Cheng et al. have employed a three-element analytical model of flat-ended punch indentation to describe a polymer's viscoelastic properties¹⁶. Ngan et al. used a linear viscoelasticity model to uncover the details of the unloading portion of an indentation curve where a nose appears¹³. Shortly

^a Center for Renewable Carbon, University of Tennessee, 2506 Jacob Drive, Knoxville, TN, 37996.

^b Department of Materials Science and Engineering, University of Tennessee, Knoxville, TN 37996, USA.

^c SEMS, 3M Company, St. Paul, MN, 55119, USA

^d Forest Products Laboratory, USDA Forest Service, Madison, WI, USA

*Corresponding author. Tel: +1 865-946-1120; fax: +1 865-946-1129
Email: swang@utk.edu

after, they proposed a creep correction procedure based on power-law to successfully calculate the contact stiffness from commercial nanoindentation data, and they validated the formula by finite element analysis (FEM) simulation and by experiment¹⁷. Schiffmann summarized and compared four rheology models using nanoindentation creep and stress relaxation tests to describe the viscoelastic behaviour of polycarbonate¹⁸. Liu et al. developed a model based on the Burgers viscoelastic concept and made a correlation between nanoindentation data and the viscoelastic behaviour of a polymer material¹⁹. Oyen et al. expanded a viscoelastic-plastic (VEP) model to predict the indentation response of time-dependent materials by incorporating viscous, elastic, and plastic elements²⁰. Liu et al. investigated the displacement of the tip during loading and the onset of unloading by indentation performed on a polymer material, showing that the derived solution consisted of elastic, viscous and plastic deformation¹⁹.

Wood is a complex composite with many components. It displays viscoelastic behaviour and also has water-sensitive properties. The mechanical and creep behaviour of wood subjected to diverse relative humidity environments has been widely studied experimentally and theoretically at the macro scale²¹⁻²⁴. Mukudai proposed a viscoelastic bending model to interpret the characteristics of viscoelastic wood under moisture change cycles based on a hypothesis that there exists a slippage between the S_1 and S_2 layers when wood is in the process of drying²⁵. Padanyi predicted the difference between moisture-accelerated creep and constant relative humidity creep, a difference that depends on the amount of free volume in the fiber. It is now clear that moisture content has a negative effect on the stiffness and strength of bulk wood and wood cell wall below a saturated moisture content²⁶. On the specific question of how the three main components in the cell wall respond to varying moisture contents, a number of reports have demonstrated that hemicelluloses are more sensitive to moisture content than are celluloses and lignin²⁷. However, studies of how moisture content affects the viscoelastic properties of wood cell wall at the submicron-scale have been limited. In the current study, we performed nanoindentation tests on the S_2 layer of wood cell wall and calculated the creep compliance of wood cell wall subjected to various moisture contents. The viscoelastic properties of wood cell wall in various relative humidity conditions were investigated based on the Burgers model and the Generalized Maxwell viscoelastic concept. The parameters presented in the Burgers model are discussed. Finite element analysis (FEA) was conducted based on the Generalized Maxwell model and correlated with the nanoindentation experiments. As

an extension of the experiments, the stress evolution due to the visco effect was obtained via FEA.

Experiment Procedures

Materials

Loblolly pine (*Pinus taeda* L.) was obtained from southern Arkansas and Tennessee. A loblolly pine disk was cut 30 cm above the ground from a tree. The 32nd annual ring was picked with the late wood located in the apex of the block. The microfibril angle was measured to be 31 degrees. Two sample preparation methods, with and without epoxy resin, were used in this research. The sample without embedding medium was used to investigate the cell wall swelling. A wood sample was cut into a block 8 mm in length, 8 mm in width, and 15 mm²⁸ in height. Four pieces of wood block with late wood located on the same annual ring were picked and cut into small blocks 1 mm in width, 1 mm in thickness, and 5 mm in length. Samples were embedded into epoxy resin without the influence of resin penetration into wood cell wall. The detailed sample preparation procedure has been discussed in our previous research²⁹. In brief, a cross-section of wood cell wall was polished by an ultramicrotome equipped with a diamond knife. A smooth and well-polished surface with roughness less than 0.5 nm was obtained to ensure good contact. Samples were ready for performing indentation after being fixed to an aluminium mounting holder³⁰. Industrial-grade glycerin solution (ASTM® D6584 Glycerin solution, Sigma Aldrich, MO, USA) and desiccant were used to control the relative humidity inside the chamber.

Control of humidity in small environment chamber

Inside the indentation chamber, the relative humidity to which samples needed to be subjected was maintained constantly and adjusted by using various aqueous glycerin solutions. All glycerin solutions were maintained at a constant laboratory temperature of 23 ± 2 °C. Samples were stored in a pre-sealed TriboIndenter chamber and exposed to the environment 24 hours before the indentation test. The moisture content in wood is ordinarily expressed as a fraction of the water mass and the mass of the oven dry wood³¹. Oven-dry weight (samples were dried in an oven set at 103 ± 2 °C) and weight under each relative humidity (RH) were used to determine the percentage of moisture content according to Eq. 1:

$$MC = (G_g - G_{od}) / G_{od} \times 100\% \quad (1)$$

where G_g is the green mass of wood and G_{od} is the oven-dry mass.

For indentations performed in water, each wood sample was stored in a specially designed aluminum holder filled with water throughout testing. For each wood sample, nanoindentation tests were finished within two hours to minimize the variation of structure/mechanical properties. The relative humidity was monitored using a hygrometer. The specimens, denoted as A, B, C and D were conditioned in an oven, 18% RH, 37% RH and in water separately. The corresponding moisture contents of each sample were calculated to be 0%, 6%, 18% and 110%.

Measurement of wood cell wall hardness and elastic modulus by nanoindentation

Nanoindentation tests were performed using a Hysitron TriboIndenter system (Hysitron, Inc., Minneapolis, MN) equipped with a Berkovich indenter, which is a three-sided pyramidal point with a known area-to-depth function¹². The fluid cell tip, which is a standard Berkovich tip mounted on a long shaft, was used through the test. The extended shaft, approximately 4 mm in length, allowed the end of the probe to be completely immersed in a liquid, while the probe holder and transducer remained in the air. When underwater indentation was performed, the tip approached the surface of the targeted cell wall with the sample partially immersed in the water. Water was added after this operation to fully cover the cell wall. A closed-loop feedback control was selected to accurately identify the sample surface, which is very important for shallow indentations. At each relative humidity, at least 25 tests were conducted with the fluid cell tip in load control and using a constant loading rate at room temperature. The trapezoidal load function was set up at maximum load $P_{\max} = 250 \mu\text{N}$, with loading, holding and unloading times of 5 s, 5 s and 2 s, respectively. The holding times were set up, firstly, to avoid the effect of creep occurring in the viscous material during the unloading¹⁹; and secondly to investigate the viscoelastic properties of the cell wall.

The configuration of the scanning probe microscopy (SPM) assembly in the TriboIndenter system makes it capable to accurately position the wood cell walls' S₂ layer. By scanning the cell wall's cross-section surface, interesting indent positions were marked on the SPM image. Indents were implemented and checked before and after scanning. Only indents in the middle of cell wall's S₂ layer were selected as valid data. Indents performed in the embedding epoxy or in the borders of cell walls were discarded. The load-displace curves that were obtained were used to calculate the reduced modulus E_r and hardness H based on Oliver and Pharr's method (Eqs. (2) and (3)). The reduced modulus E_r was obtained from unloading slope

dP/dh evaluated at 70-90% of the maximum load P_{\max} ; the hardness H was calculated by the maximum load and project contact area A_{hc} at peak load¹².

$$E_r = \frac{\sqrt{\pi}(dP/dh)_{\text{unloading}}}{2\sqrt{A_{hc}}} \quad (2)$$

$$H = \frac{P_{\max}}{A_{hc}} \quad (3)$$

where P is the indentation load and A_{hc} is the projected contact area.

Rheological models

Viscoelastic material during nanoindentation

Viscoelastic material exhibits both viscous and elastic behaviour. For the linear elastic properties, the material reacts as a spring and deformation will recover to its original dimensions when stress is removed. This could be described by Hooke's law:

$$\sigma = E \cdot \varepsilon \quad (4)$$

where E is the elastic modulus. in nanoindentation case, the deformation is not a pure shear deformation but a complex superposed normal and shear deformation. However, the material retains the relationship between σ and ε no matter the type of deformation. On the other side, the viscous component is modeled as a dashpot, which is analogous to the energy dissipation. The stress and strain rate relationship can be expressed as follows:

$$\sigma = \eta \cdot d\varepsilon / dt \quad (5)$$

in which η is the viscosity of a material and $d\varepsilon/dt$ is the time derivative of the strain.

For a creep test, the stress is held constant, $\sigma = \sigma_0$, so the creep compliance $J(t)$ is defined by the following:

$$J(t) = \varepsilon(t) / \sigma_0 \quad (6)$$

The load P , contact area A and indentation depth h are three important parameters in nanoindentation. The tip used in all experiments was a pyramidal indenter (Berkovich tip). Kirsten Ingolf Schiffmann¹⁸ has mentioned in his research that the representative stress is given by $\sigma = P/A$, and that the representative strain is defined by the following:

$$d\varepsilon = \cot \delta \cdot \frac{dh}{h} \quad (7)$$

thus the creep compliance is given by:

$$J(t) = \frac{1}{c} \frac{A(t)}{P_0} \quad (8)$$

where $c = 2(1 - \nu^2) \tan \delta$, ν is the Poisson ratio, and δ is the half opening angle of the indenter (70° in Berkovich). Load $P = P(0)$ was able to be obtained directly by the instrument. However, the contact area $A(t)$ had to be calculated by the area function of the tip, which is described by a polynomial:

$$A = C_0 h_c^2 + C_1 h_c + C_2 h_c^{1/2} + C_3 h_c^{1/4} + C_4 h_c^{1/8} + C_5 h_c^{1/16} \quad (9)$$

where C_i is the tip constant and h_c is the contact depth, which can be related to the maximum indentation depth h_{\max} in Oliver and Pharr's method by the following:

$$h_c = h_{\max} - \alpha \frac{P}{S} \quad (10)$$

where α is the geometrical constant and S is the contact stiffness, which can be derived from dP/dh .

In the creep test, the holding load is constant and the contact area changes with time. Thus, h_c is given by

$$h_c(t) = h(t) - \alpha \frac{P_0}{S_f} \quad (11)$$

where $h(t)$ is the actual indentation depth during the holding period and S_f is the final stiffness calculated from the unloading segment.

Burgers model and Generalized Maxwell model

For different viscoelastic materials, various models, including the Maxwell model and the Kelvin-Voigt model, were developed to predict the deformation of different viscoelastic materials¹⁸. In our analysis, both the Burgers model and the Generalized Maxwell model were applied to rationalize the experimental results and to investigate the wood cell wall with different humidities separately.

With reference to the Burgers model, a combination of Maxwell and a Kelvin element were taken into consideration with the schematic diagram shown in Fig. 1(a). The Maxwell element is represented by a purely viscous damper and a purely elastic spring connected in series. The Kelvin element is a purely viscous damper and a purely elastic spring connected in parallel. The relationship between stress σ and the deformation ε of the viscoelastic material is given by the following:

$$\sigma + p_1 \dot{\sigma} + p_2 \ddot{\sigma} = q_1 \dot{\varepsilon} + q_2 \ddot{\varepsilon} \quad (12)$$

where $\dot{\sigma}$, $\ddot{\sigma}$, $\dot{\varepsilon}$, $\ddot{\varepsilon}$ are defined as the first and second time derivatives of stress and deformation and can be expressed as

$$p_1 = \frac{\eta_1}{E_e^B} + \frac{\eta_1}{E_d^B} + \frac{\eta_2}{E_d^B} \quad p_2 = \frac{\eta_1 \eta_2}{E_e^B E_d^B} \quad (13)$$

$$q_1 = \eta_1 \quad q_2 = \frac{\eta_1 \eta_2}{E_d^B}$$

where E_e^B , E_d^B are the spring constants and η_1 , η_2 are viscosities in Fig. 1(a).

The stress σ is constant in the case of the creep test, so the first and second derivatives of stress are zero. Consequently, the Eq. (12) can be constructed into

$$\sigma = q_1 \dot{\varepsilon} + q_2 \ddot{\varepsilon} \quad (14)$$

By applying this equation to Equation (6), the creep compliance formula, a solution can be written as the form of creep compliance:

$$J(t) = J_0 + J_1 \cdot t + J_2 [1 - \exp(-t/\tau_0^B)] \quad (15)$$

where $J_0 = 1/E_e^B$, $J_1 = 1/\eta_1^B$, $J_2 = 1/E_d^B$ and $\tau_0^B = \eta_2^B/E_d^B$. Here τ_0^B is the retardation time, which describes the retarded elastic deformation of the Kelvin model in the Burgers model, and it is an important parameter that reflects the viscoelastic properties of a material.

The Generalized Maxwell model is another of the most general forms of linear models of viscoelasticity. With $n + 1$ constituent elements in parallel, n Maxwell models and one isolated spring element to warrant solid behaviour in parallel as shown in Fig. 1(b), the combination can simulate the viscoelastic properties of many different materials³².

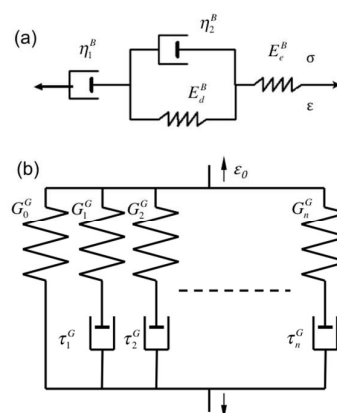


Fig. 1. Schematic images of (a) four-element Burgers model and (b) Generalized Maxwell Model.

It is clear that the shear modulus $G(t)$ decreases with time as follows:

$$G(t) = g_R(t)G_0 \quad (16)$$

where $g_R(t)$ is the a time-dependent dimensionless relaxation modulus, only related to time t , and G_0 is the instantaneous shear modulus. The dimensionless relaxation modulus can be expressed by an N -terms Prony series expansion.

$$g_R(t) = 1 - \sum_{i=1}^N g_i^G (1 - e^{-\frac{t}{\tau_i^G}}) \quad (17)$$

in which τ_i^G is the retardation time for i^{th} dashpot and g_i^G is the material constant to represent the influence of the i^{th} Maxwell element. For early time ($t \ll \tau_i$), $g_R(t) = 1$, and the shear modulus is G_0 which means that all the dashpots are frozen and cannot move. After that, $g_R(t)$ is gradually decreased and finally reaches the long-term shear relaxation modulus G_∞ . For more details of the Generalized Maxwell model, we refer the reader to the Abaqus documentation collection³³.

Results and Discussion

Effects of moisture content on the elastic modulus and hardness

The nanoindentation load-displacement curves (P - h curve) for Samples A, B, C and D, with the same loading and unloading rates and with constant holding times at peak load, are plotted in Fig. 2(a), which includes a comparison of the wood cell walls at different moisture contents. Obvious differences among the indentation responses of the four samples include the displacements during the loading and holding segments. When the moisture content was high, the curves shifted from the left-hand to the right-hand and caused an increase in penetration depths at the end of loading, residual displacement, and displacement during the constant holding segment. Atomic force microscope images in Fig. 2(b) illustrate the residual indentation marks after unloading. There was no distinct size change in the residual marks between Samples A and B. However, obviously larger indent marks were clearly seen on Sample C and vaguely identified on Sample D under wet conditions.

Fig. 3 illustrates the relationship between moisture content and elastic modulus/hardness in the longitudinal direction of the wood cell wall. The trends highlighted by these two figures show that moisture content has a negative effect on both the elastic modulus and hardness; this can be inferred from the box-and-

whisker plots in Fig. 3. The samples have more variation in elastic modulus than they do in hardness. All pairwise comparisons of the mean values of the wood cell walls' elastic modulus and hardness under moisture content were conducted by the Student's t -test. Statistical analysis (connecting letters report shown in insert of Fig. 3(a) and (b)) using the Student's t -test further revealed that significant differences existed

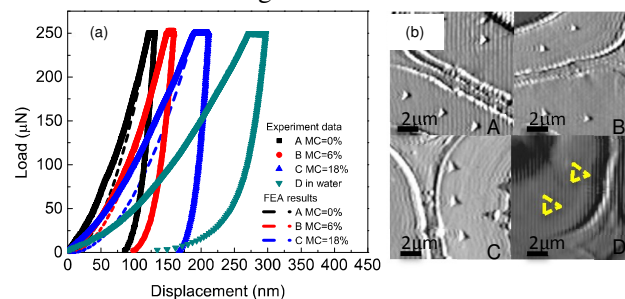


Fig. 2. (a) Typical indentation curves with fluid cell indenter at different moisture contents with a peak load of 250 μN and 5 s holding time at maximum load for creep; (b) Atomic force microscope image showing the residual indentation marks on cell walls. In D, the triangles show residual indentation marks.

among different conditions. The percentage reduction of the modulus from the oven-dried state to the 18% moisture content was 32.4%. The percentage reduction of hardness from the oven-dried state to the 18% moisture content state was 46.7%. Those trends agree well with Kojima's results, which illustrated the phenomenon of moisture-content dependence and were verified by simulation experiments³⁴.

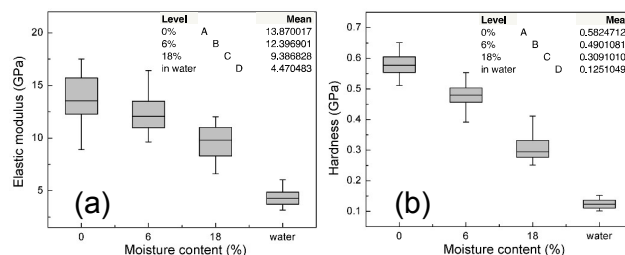


Fig. 3. Effect of moisture content on (a) elastic modulus and (b) hardness of wood cell wall. Figures at top right in each graph show the connecting letter report for Student's t comparison between each pair. Levels not connected by same letter are significantly different.

The effects of moisture content on nanoindentation displacement rate were investigated and results are presented in Fig. 4. The nanoindentation displacement rate could be described as Eq. $\dot{h} = dh/dt$, where h is the instantaneous indenter displacement and t is time³⁵. We plotted the data separately for two regions of loading and holding. In the indentation's rising region, the displacement rate diminished significantly under all moisture contents with the same amount of

applied force and time. As the moisture content increased, the indentation displacement rate underwent rapid increase as well, resulting in a large number. It is also evident from Fig. 4(b) that the displacement rates under all moisture contents had the tendency to become constant after 6 seconds. These observations indicate that high moisture content leads to softening of the wood cell wall, which consequently weakens the mechanical properties of the cell wall.

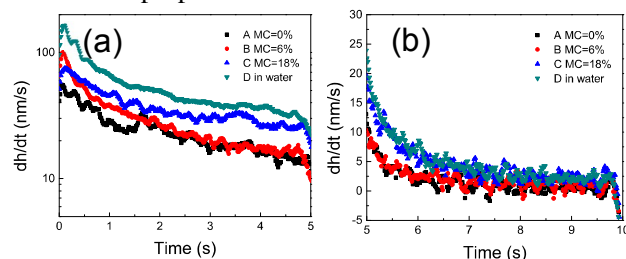


Fig. 4. Indentation creep rate as a function of time with different moisture content under nanoindentation with a Berkovich indenter (a) during indentation 5 seconds rising; (b) during indentation creep under a fixed load of 250µN.

Cell wall swelling

An interference microscope with a dimension readout function in the SPIP system was used to investigate the cell wall's swelling behaviour as affected by water. The cell wall's line profile and the 3D surface topography are plotted in Fig. 5. An obvious dimension change (1.7143 µm in thickness difference) was detected between the air-dry sample and the wet sample. The amount of amorphous area and the number of dissociative hydroxyl groups dominated the cell wall's water absorption ability³⁶. It has been demonstrated that large amounts of hydroxyls and other oxygen-containing groups exist in amorphous cellulose, and that hemicellulose and lignin have the ability to attract water³⁷. When the water is introduced, dissociative hydroxyl groups in the amorphous area start to attract water molecules. The original hydrogen bonds existing in the amorphous region of the wood constituents are broken, causing the formation of new hydrogen bonds between water molecular and hydroxyl groups, increasing the distance between molecule chains, and consequently leading to the expansion of the cell wall in the transverse direction. The swelling of the wood cell wall leads to a decrease of cellulose microfibril numbers per unit area underneath the indentation; consequently, the stiffness of the wood cell wall is reduced.

Wood cell wall's ultrastructure can be described as one of complicated fiber-reinforced composites, wherein hierarchically oriented microfibrils are surrounded by a matrix of hemicellulose and lignin. Typically, in the S₂ layer, the thickest part of secondary cell wall layer where these nanoindentations were

performed, it has been argued that cellulose microfibrils aggregate into fibril bundles and are mainly surrounded by amorphous hemicellulose, xylan, glucomannan and lignin. However, it is evident that only the hemicellulose has a pronounced effect on the mechanical properties of moist wood³⁸. Hemicellulose has the strongest water absorption ability in the cell wall due to its structure and distribution in the natural cell wall. It is now clear that hemicellulose in the S₂ layer continuously surrounds the cellulose microfibril, preferentially oriented along the cell wall axis. In addition, the hemicellulose has a random, amorphous structure with little strength. The negative linear relationship between moisture content and the glass transition temperature (T_g) of hemicellulose indicates that high moisture content (moisture content=20%) dramatically drags the T_g down to room temperature, in contrast to the high T_g of 150 to 220 °C under dry conditions³⁹. In the case of wet conditions where cell wall is subject to varying moisture contents, numerous spherical water molecules are initially stored in the expanded volume caused by the cell wall's swelling. When nanoindentation is performed, the aforementioned water molecules existing in the wood cell wall underneath the indenter make the indenter easier to push into the material. For this reason, water acts as a cause of plasticizer in wood cell wall by softening the hemicellulose and the amorphous cellulose.

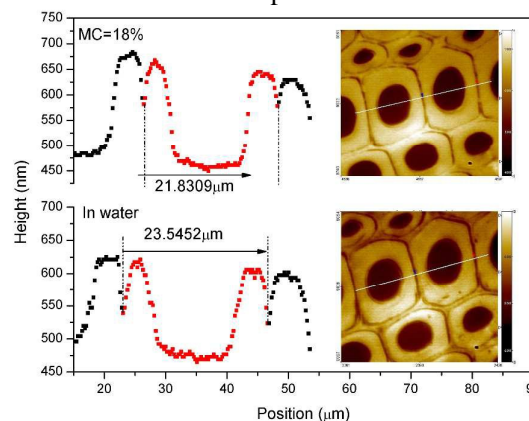


Fig. 5. Line profile and optical micrograph of air-dried and wet loblolly pine cell wall using interference surface mapping microscope.

Effect of moisture content on creep behavior via Burgers model

The viscoelastic behaviour of wood cell wall was investigated by fitting the calculated creep compliance to the viscoelastic Burgers model. The benefit of this model is that fit parameters can be interpreted physically as an instantaneous elastic deformation,

followed by a viscoelastic deformation and a viscous deformation. Based on Burgers model, ideally, the stress-strain-time behaviour of a material is modelled in when the material is subjected to a constant stress over time plus an initial strain. Hence, the investigation was restricted to 5 s of creep and the parameters were determined by means of the indentation holding data. Fig. 6 shows the experimental creep compliance data on wood cell wall with varying moisture content, together with Burgers model predicted creep compliance, shown in red lines. The comparative study of viscoelastic behaviour shows excellent agreement, with a high correlation coefficient of 0.99, indicating that Burgers model is appropriate for predicting the wood cell wall's viscoelastic behaviour. The creep compliance at the onset of unloading increased from 0.265 1/GPa in the oven-dried condition to 1.12 1/GPa under water. The creep compliance percentage increased during the 5 s; creep compliance percentage is, defined as the compliance differences between the beginning and ending of the holding period, divided by the creep compliance at the beginning of holding. These were compared among the four samples. Results showed that creep compliance percentage increased 9.0%, 12.1%, 17.8%, and 17.0% for Samples A, B, C, and D, respectively. In other words, the samples with higher moisture content deformed more when subjected to the constant load.

In a polymer chain, the induction of moisture content tends to increase the number of water molecules at the interface between amorphous hemicellulose and crystal cellulose and to enlarge the inter-chain distance, which weakens the structural continuity and reduces the resistance of the wood cell wall to creep.

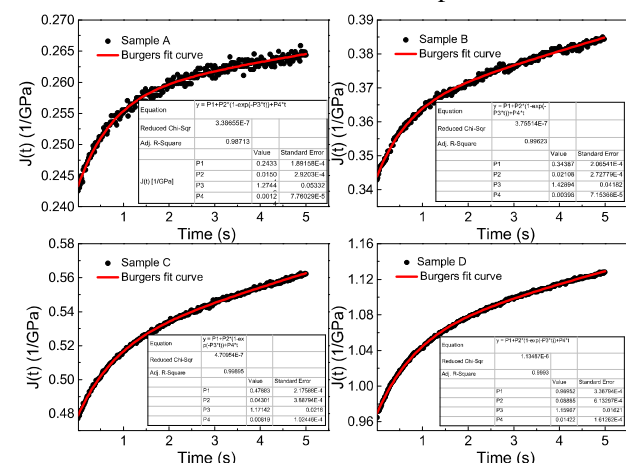


Fig. 6. Creep Compliance $J(t)$ and Burgers model fit (red line) of wood cell wall (a) Sample A with moisture content of 0% (b) Sample B with moisture content of 6% (c) Sample C with moisture content of 18% (d) Sample D in water.

Simulated results using the Burgers model

The viscoelastic behaviour of wood cell wall in terms of stress and strain can be described by the four-parameter Burgers model by means of the observed $J(t)$. The parameters in Burgers model include E_e^B , E_d^B , η_1^B , η_2^B and τ_0^B : modulus of elasticity, modulus of viscoelasticity, coefficients of plasticity, viscoelasticity, and retardation time, respectively, which were obtained by fitting the creep compliance curve to Eq. (15). The effects of moisture content on the viscoelastic behaviour in terms of the fitting parameters are plotted in Fig. 7. Apparently, the viscoelastic behaviour is sensitive to the moisture content. It was observed that in the moisture range of the current study, parameters E_e^B , E_d^B , η_1^B and η_2^B scale coincided almost linearly with moisture. Wood cell walls immersed into water were found to have the lowest values for the four parameters fitted from Burgers model of any of the cell walls under varying moisture content conditions. A similar trend has been observed in the tensile creep behaviour of wood²².

The Young's modulus can be converted from the reciprocal start value of creep compliance using $E = 2(1 + \nu)/J(0)$. The estimated Young's moduli from Burgers model for various moisture contents are summarized in Table 1. These values are smaller than the Young's modulus obtained from Oliver and Pharr's standard method. This is to be expected, since, according to the solution in Eq. (8), creep compliance is directly proportional to the contact area, which is related to the square of displacement at the onset of holding. In fact, the 5 s loading during nanoindentation induced a large starting displacement, consequently shifting the

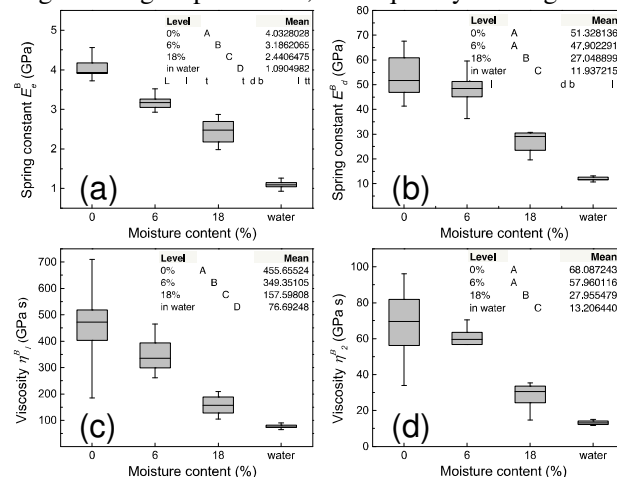


Fig. 7. Effect of moisture content on the fitted parameters from Burgers model (a) spring constant E_e (b) spring constant E_d (c) viscosity η_1 and (d) viscosity η_2 ; Note: Figures in the upper right corner show letter report for Student's t comparison between each pair. Levels not connected by same letter are significantly different.

creep compliance curves up and leading to the decrease of Young's modulus. In spite of the value decreasing, the effect of moisture content was still pronounced and consistent with the conclusions from Oliver and Pharr's calculation.

Table 1. Comparison of Young's modulus calculated from different methods

Moisture content (%)	Creep compliance (1/GPa)	E^* from Burgers model (GPa)	E from O-P method (GPa)	E from the Generalized Maxwell model (GPa)
0	0.25	10.5	13.9	14.4
6	0.31	8.3	12.4	11.5
18	0.4	6.3	9.4	9
water	0.91	2.9	4.5	N/A

E^* : Young's modulus calculated from Burgers model is based on holding segment when $t=5-10$ s.

Retardation time spectrum

The creep behaviour of viscoelastic material during creep test exhibits creep compliance that can be described in terms of continuous retardation multiplied by the spectrum $L(\tau)$. Accordingly, the retardation time spectrum resulting from the creep compliance is given by:

$$L(\tau) \approx +t \left. \frac{dJ(t)}{dt} \right|_{t=\tau} \quad (18)$$

The details of this formula's derivation are described in¹⁸. The curve plotted using Eq. (18) can be directly compared with experimental data as shown in Fig. 8. The result clearly shows that Burgers model yields a good approximation of the experimental time spectrum, with one single peak predicted at the first second of holding, although there exists a small variation. In fact, the time at the single peak represents the retardation time τ_0 , which is associated with the parallel spring-dashpot system in Burgers model. The Burgers model yields an average retardation time of 1.36 s, 1.21 s, 1.09 s and 1.12 s at each moisture content, ranging from the oven-dry state to the in-water state. A negative trend for the retardation time was observed for wood cell walls that were subjected to raised moisture content in air. This observation is consistent with the negative trend obtained from longitudinal tensile creep tests in other research²². In addition, the values seem to keep decreasing until they approach a plateau value around 1.1s, where water starts to dominate the viscoelastic property.

Finite Element Analysis

In order to further interpret the test results from the nanoindentation that was presented in previous section and in order to establish a relationship between the wood cell wall properties and the indentation response, a finite element analysis (FEA) was carried out using a rigid body Berkovich indenter with a cone

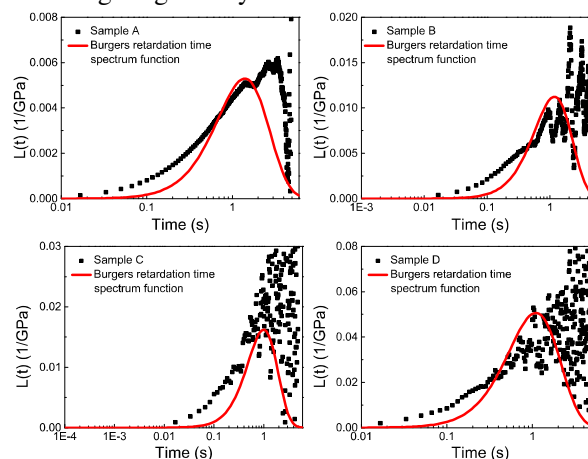


Fig. 8. Retardation time spectrum calculated from numerical differentiation of creep compliance overlaid with time spectrum derived from the analytical expression of Burgers model

semi-angle at 70.3° . The boundary value problem was resolved with the commercial finite element package ABAQUS 6.10 (3DS SIMULIA)³³. An axisymmetric model was used in the simulation due to the load condition, the boundary condition, geometry features, and constitutive behaviour of wood, as shown in Fig. 9. The area close to the contact area was finely meshed and the fine mesh was migrated to a coarse one. Contact between the indenter and the wood sample was assumed to be frictionless. Following the real experiment in the lab, the deformation had two successive steps: applying 250 μ N loads for 5 s and holding the load for 5 s to fit the $P-h$ curve and to obtain the material parameters of the wood samples at different moisture contents and evaluate the stress. The bottom of the wood sample was fixed (i.e. $u_i = 0, i = 1, 2, \dots, 6$). Considering that the size of the cell wall is significantly larger than the size of the indenter contact area in the experiment, the deformation was quite localized and the boundary effect was negligible. As a result, the depth of sample in the simulation was more than 10 times the displacement of the indenter, in order to eliminate the boundary effects. A load along the symmetrical axis was applied on the indenter and the remaining five degrees of freedom were fixed. The significant advantage of the axisymmetric analysis was that the computational cost was substantially reduced without losing accuracy, compared with a fully three-dimensional analysis.

To deal with the previously stated significant size difference between indenter and sample, the wood cell wall in simulation was considered to be an isotropic viscoelastic according to the Generalized Maxwell model. For plant materials, there are two different relaxation behaviours that have been observed in

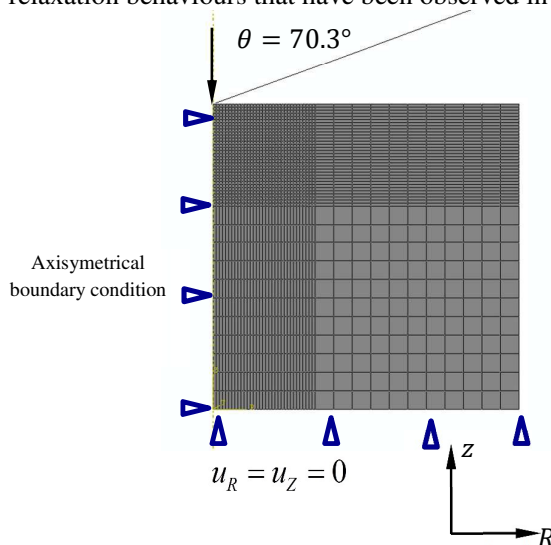


Fig. 9. Mesh pattern, boundary condition and load condition used for axisymmetric finite element modeling of nanoindentation process.

experiments: a quick relax mode (low frequency) and a slow relax mode (high frequency)⁴⁰. Therefore, the dimensionless relaxation modulus in Eq. (17) can be expressed as:

$$g_R(t) = 1 - g_1^G \left(1 - e^{-\frac{t}{\tau_1^G}}\right) - g_2^G \left(1 - e^{-\frac{t}{\tau_2^G}}\right) \quad (19)$$

For simplicity, following suggestions in previous literature, it was assumed that the two modes have almost the same influence on the decay of the shear modulus (i.e. $g_1 = g_2 = 0.5$)⁴¹. For this reason, finite element analysis was used to determine three parameters, G_0 (or E_0 for $E_0 = 2G(1+\nu)$), τ_1 and τ_2 , which link the indentation response parameter with the material properties, by fitting the $P-h$ curves. In fact, only the $P-h$ curves of Samples A, B and C were successfully fitted. Fig. 2 shows that Sample D's (in-

water) $P-h$ curve shape exhibits significant differences from the other three curves, with a nearly linear loading curve. This implies that wood cell wall immersed in water behaves more like a fluid than a solid. Despite the fact that the Generalized Maxwell model contains dashpots, which is the mechanical analog for a Newtonian fluid, the whole model is based on the assumption of solid mechanics. Consequently, that model fails to catch the essence of the pure fluid and was found to be inappropriate for the case of Sample D.

The parameters obtained via simulations are listed in Table 2. It is of interest to note that the instantaneous elastic module was dependent on the moisture content. Values decreased from 14.4 GPa to 9 GPa with the increase in moisture content. A similar trend was observed for the relaxation time (both τ_1 and τ_2). It can be speculated that wood cell wall under low moisture content is harder in the loading region but has a better ability to resist the further deformation in holding region, which is consistent with experimental observation. Moreover, the calculated values from FEA are consistent with ones from Oliver and Pharr's method.

Table 2. Summary of fitting parameters from Generalized Maxwell model using FEA

Moisture content (%)	E_0 (GPa)	τ_1 (s)	τ_2 (s)
0%	14.4	0.13	45
6%	11.5	0.05	30
18%	9	0.01	16

To further correlate the moisture content with the cell wall's ability to creep, the stress evolution during the time at constant load was investigated. Von Mises stress distributions at $t=10$ s, normalized by the maximum of von Mises stress at $t=5$ s, are presented in Fig. 10 and compare the three conditions in Figs. 10 (a), (b) and (c). It can be easily observed that the decay of stress was greatest in Sample C with a value of 80.93%, followed by Sample B with a value of 88.5%, and Sample A with a value of 92.02%. This trend implies

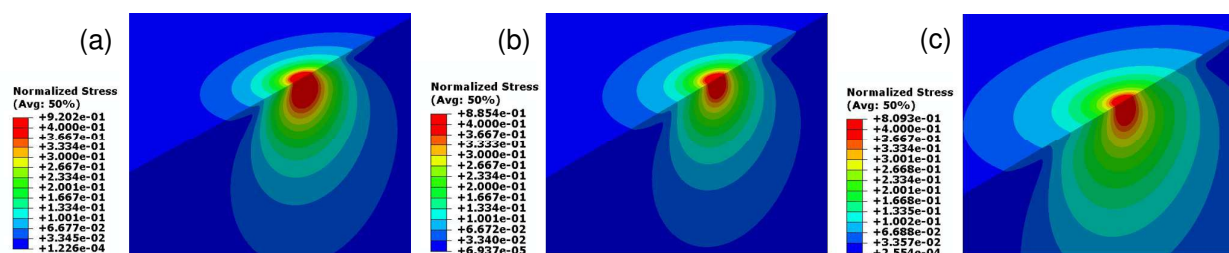


Fig. 10. Normalized stress distributions at the onset of unloading ($t=10$ s) (a) dry wood (b) 6% moisture content (c) 18% moisture content (the axisymmetrical results are swept into full three-dimensional contour),

that the dry sample has better creep resistance, which agrees with our previous experimental analysis.

Conclusions

Water is considered to be the cause of a plasticizer to soften and thicken wood cell wall and it makes it easy to break the hydrogen bonds between microfibrils which leading to a decrease in the cell wall's mechanical properties. Nanoindentation was performed on wood cell wall to investigate the effects of moisture content on the mechanical and rheological properties of the cell wall. Negative relationships between instantaneous elastic modulus/hardness with moisture content were experimentally observed from indentations in the cell walls. Based on the viscoelastic concept, the moisture dependence of wood cell creep were investigated using Burgers model and the Generalized Maxwell model. The parameters with physical interpretation extracted from both models were validated to be sensitive to moisture content. The microstructure analysis on the moisture-dependent creep agreed well with the model simulation, from which parameters were extracted to explain the rheological properties of the wood cell wall. Retardation time spectra were determined from creep compliance calculated from experiment results and were found to yield a good approximation with the fitted spectra obtained from Burgers model. The elastic and viscous parameters tended to decrease with increasing moisture content. In all, both Burgers model and Generalized Maxwell model are proved to be appropriate for investigating moisture dependence of wood cell wall's viscoelastic creep. In spite of the fact that Burgers model worked well in predicting wood cell wall's viscoelastic behaviour, the calculated elastic modulus from fitting parameters exhibited smaller values compared with Oliver and Pharr's method, due to the creep phenomenon observed during the loading segment of the nanoindentation. FEA with Generalized Maxwell model was applied to overcome this problem. Its simulation yielded similar results to that using Burgers model but with more accurate approximation of the elastic modulus.

Acknowledgements

The Authors gratefully acknowledge financial support by the Zhejiang Key Level 1 Discipline of Forestry Engineering, Wood Utilization Grant and Forest Products Lab at Madison, the support of this research by USDA Special Wood Utilization Grants R11-0515-041 and R11-2219-510, the University of Tennessee, Department of Forestry, Wildlife and Fisheries, Center for Renewable Carbon, and the

Agricultural Experiment Station McIntire-Stennis Grant TENOOMS-101.

References

1. Q. Wu, Y. Meng, K. Concha, S. Wang, Y. Li, L. Ma and S. Fu, *Industrial Crops and Products*, 2013, **48**, 28-35.
2. C. Liao, Y. Deng, S. Wang, Y. Meng, X. Wang and N. Wang, *Wood and Fiber Science*, 2012, **44**, 63-70.
3. X. Wang, Y. Deng, S. Wang, C. Liao, Y. Meng and T. Pham, *Bioresources*, 2013, **8**, 1986-1996.
4. Y. Wu, S. Wang, D. Zhou, C. Xing, Y. Zhang and Z. Cai, *Bioresour. Technology*, 2010, **101**, 2867-2871.
5. X. Li, S. Wang, G. Du, Z. Wu and Y. Meng, *Industrial Crops and Products*, 2013, **42**, 344-348.
6. C. Xing, S. Wang and G. Pharr, *Wood Sci. Technol.*, 2009, **43**, 615-625.
7. M. A. Ermeýdan, E. Cabane, N. Gierlinger, J. Koetz and I. Burgert, *RSC Advances*, 2014, **4**, 12981-12988.
8. A. Jäger, K. Hofstetter, C. Buksnowitz, W. Gindl-Altmutter and J. Konnerth, *Composites Part A: Applied Science and Manufacturing*, 2011, **42**, 2101-2109.
9. L. Zou, H. Jin, W.-Y. Lu and X. Li, *Materials Science and Engineering: C*, 2009, **29**, 1375-1379.
10. S. H. Lee, S. Wang, G. M. Pharr, M. Kant and D. Penumadu, *Holzforchung*, 2007, **61**, 254-260.
11. S. H. Lee, S. Wang, G. M. Pharr and H. T. Xu, *Composites Part A: Applied Science and Manufacturing*, 2007, **38**, 1517-1524.
12. W. C. Oliver and G. M. Pharr, *Journal of Materials Research*, 1992, **7**, 1564-1583.
13. A. H. W. Ngan and B. Tang, *Journal of Materials Research*, 2002, **17**, 2604-2610.
14. J. Zhang, C. Wang, F. Yang and C. Du, *RSC Advances*, 2014, **4**, 41003-41009.
15. E. Lee and J. R. M. Radok, *Journal of Applied Mechanics*, 1960, **27**, 438-444.
16. L. Cheng, X. Xia, W. Yu, L. E. Scriven and W. W. Gerberich, *Journal of Polymer Science Part B: Polymer Physics*, 2000, **38**, 10-22.
17. A. H. W. Ngan, H. T. Wang, B. Tang and K. Y. Sze, *International Journal of Solids and Structures*, 2005, **42**, 1831-1846.
18. K. I. Schiffmann, *Int. J. Mater. Res.*, 2006, **97**, 1199-1211.
19. C. K. Liu, S. Lee, L. P. Sung and T. Nguyen, *J. Appl. Phys.*, 2006, **100**, 9.
20. M. L. Oyen and R. F. Cook, *Journal of Materials Research*, 2003, **18**, 139-150.
21. C. Skaar, *Wood-water relations*, Berlin Heidelberg New York., 1988.
22. Y. Kojima and H. Yamamoto, *J. Wood Sci.*, 2005, **51**, 462-467.
23. C. Takahashi, Y. Ishimaru, I. Iida and Y. Furuta, *Holzforchung*, 2006, **60**, 299-303.
24. H. Qing and L. Mishnaevsky, *Computational Materials Science*, 2009, **46**, 310-320.
25. J. Mukudai and S. Yata, *Wood Sci. Technol.*, 1987, **21**, 49-63.
26. Y. Yu, B. Fei, H. Wang and G. Tian, 2011, **65**, 121-126.
27. W. J. Cousins, *Wood Sci. Technol.*, 1978, **12**, 161-167.
28. W. T. Y. Tze, S. Wang, T. G. Rials, G. M. Pharr and S. S. Kelley, *Composites Part A: Applied Science and Manufacturing*, 2007, **38**, 945-953.
29. Y. Meng, S. Wang, Z. Cai, T. M. Young, G. Du and Y. Li, *Appl. Phys. A-Mater. Sci. Process.*, 2013, **110**, 361-369.

- 30.G. B. d. Souza, C. E. Foerster, S. L. R. d. Silva and C. M. Lepienski, *Materials Research*, 2006, **9**, 159-163.
31. *Journal*, 2007.
- 32.R. Christensen, *Theory of viscoelasticity: an introduction*, Elsevier, 2012.
- 33.Documentation and ABAQUS, *Dassault Systèmes*, 2010.
- 34.Y. Kojima and H. Yamamoto, *Wood Sci. Technol.*, 2004, **37**, 427-434.
- 35.C. Su, E. G. Herbert, S. Sohn, J. A. LaManna, W. C. Oliver and G. M. Pharr, *Journal of the Mechanics and Physics of Solids*, 2013, **61**, 517-536.
- 36.S. Zauscher, D. F. Caulfield and A. H. Nissan, *Tappi J.*, 1996, **79**, 178-182.
- 37.F. F. Wangaard, *Journal of educational modules for materials science and engineerin* 1979, **1**, 437-534.
- 38.L. Salmén, *Comptes Rendus Biologies*, 2004, **327**, 873-880.
- 39.A. M. Olsson and L. Salmen, *Acs Sym Ser*, 2004, **864**, 184-197.
- 40.D. Husken, E. Steudle and U. Zimmermann, *Plant Physiol*, 1978, **61**, 158-163.
- 41.C. M. Hayot, E. Forouzesh, A. Goel, Z. Avramova and J. A. Turner, *J Exp Bot*, 2012, **63**, 2525-2540.